

Breakup of 87 MeV ^{11}B

F. L. H. Wolfs, C. A. White, D. C. Bryan, C. G. Freeman, D. M. Herrick, K. L. Kurz,
D. H. Mathews, P. A. A. Perera, and M. T. Zanni

*Nuclear Structure Research Laboratory,
University of Rochester, Rochester, New York 14627*

(Received 14 October 1993)

A segmented focal-plane detector has been used to study the breakup of 87 MeV ^{11}B ions incident on a ^{12}C target into ^4He and ^7Li fragments at relative energies between 0 and 4 MeV. The relative energy spectra are dominated by sequential breakup of the 9.28 MeV, 10.26+10.33 MeV, and 10.60 MeV excited states in ^{11}B . The measured breakup yields decrease with increasing center-of-mass scattering angle, consistent with predictions made using single-step inelastic distorted wave Born approximation calculations. Applications of this technique to study the breakup of ^{16}O at low relative energies will be discussed.

PACS number(s): 23.60.+e, 25.40.Lw, 25.70.De, 25.70.Mn

I. INTRODUCTION

Radiative capture cross sections play an important role in the understanding of stellar burning processes and primordial nucleosynthesis. However, in the energy region of interest, it is extremely difficult to carry out direct measurements of the relevant cross sections. It has been suggested to use the inverse process, photodisintegration, measured using projectile breakup by the virtual photons provided by the Coulomb field of the target nucleus, to determine astrophysical S factors that are inaccessible by direct measurements [1].

At sufficiently high projectile energies, the two breakup products emerge with high kinetic energies and small relative angles. The coincident detection of the breakup products in the focal plane of an Enge split-pole spectrograph makes a measurement of the yield at small relative energies possible. Small relative energies of the breakup products correspond to low center-of-mass energies for the inverse reaction (the radiative capture process). Although these breakup reactions, in principle, allow us to study the inverse process at very low center-of-mass energies, the determination of the astrophysical S factor still relies on the assumption that a separation between the nuclear and Coulomb breakup processes is possible. Examples of radiative capture reactions that can be studied via projectile breakup are $^6\text{Li}(^4\text{He},\gamma)^{10}\text{B}$ and $^7\text{Li}(^4\text{He},\gamma)^{11}\text{B}$ which are important for the primordial nucleosynthesis of the B isotopes, and $^{12}\text{C}(^4\text{He},\gamma)^{16}\text{O}$, $^{14}\text{C}(^4\text{He},\gamma)^{18}\text{O}$, and $^{20}\text{Ne}(^4\text{He},\gamma)^{24}\text{Mg}$, which are important for helium burning in stars.

The use of a spectrograph to detect both breakup products has been applied by Utsunomiya *et al.* [2–4] to determine the yield for the breakup of ^7Li into ^4He and ^3H . For this reaction the mass-to-charge ratio of the beam and of the breakup products are very different, and the reaction products are well separated in the focal plane, allowing the use of two separate counters to detect the breakup products. For other breakup reactions, such as $^{16}\text{O}(\gamma,^4\text{He})^{12}\text{C}$, the mass-to-charge ratio of the beam and

of the breakup products are the same, and, consequently, these fragments are focused onto the same region of the focal plane. In this case, the use of separate counters limits the lowest relative energy of the breakup products that can be observed.

We have built a segmented focal-plane detector for the Rochester Enge split-pole spectrograph to study breakup reactions at low relative energies [5]. This focal-plane detector system was designed to measure the relative energy spectrum of the breakup products of ^{16}O down to 50 keV by limiting the size of the dead area between the two segments of the focal-plane detector to less than 3 mm.

In this paper we will discuss the first results obtained with this detector system, looking at the breakup of 87 MeV ^{11}B incident on a ^{12}C target into ^4He and ^7Li . This reaction was chosen since the reverse reaction, radiative capture of ^4He and ^7Li , has been studied in great detail at low center-of-mass energies [6]. This allows us to compare the measured breakup yields with the cross sections for radiative capture. The measured widths of the states in ^{11}B populated in the radiative capture measurements will be compared with the widths of the states observed in the relative energy spectra of the breakup products.

II. EXPERIMENTAL PROCEDURE

The measurement described in this paper has been carried out using an 87 MeV ^{11}B beam from the upgraded MP tandem accelerator of the Nuclear Structure Research Laboratory at the University of Rochester. The ^{11}B ions were incident on a 2.2 mg/cm^2 ^{12}C target. The breakup products were momentum analyzed and detected in coincidence in the focal plane of the Rochester Enge split-pole spectrograph. The aperture mounted at the entrance of the spectrograph was 0.785 cm wide and 0.927 cm high, corresponding to a solid angle of 1.2 msr. The position along the focal plane, used to determine

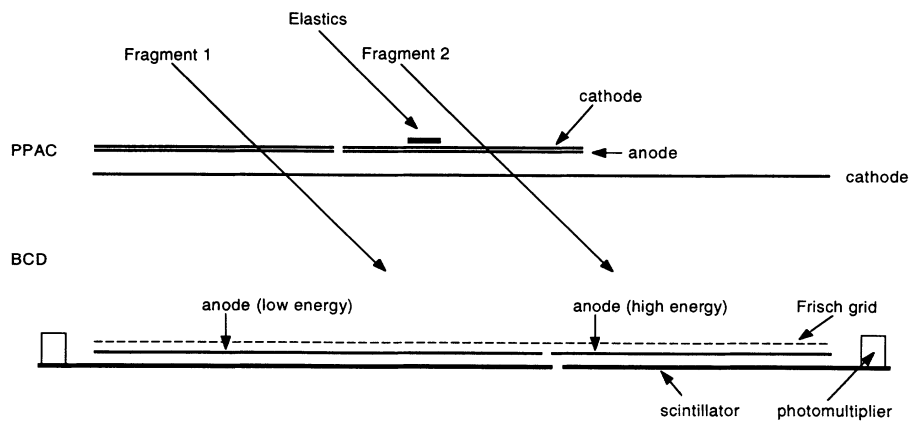


FIG. 1. Schematic view of the focal-plane detector of the Rochester Enge split-pole spectrograph. The position of the tantalum beam stop in front of the parallel-plate avalanche counter is indicated. The two arrows indicate the detection position and direction of two possible breakup products.

the kinetic energy of the reaction products, was measured using a segmented parallel-plate avalanche counter (PPAC). The nuclear charge of the reaction products was obtained using a segmented Bragg curve detector (BCD) backed by a plastic scintillator. This focal-plane detector system, described in detail in Ref. [5], is schematically

shown in Fig. 1. The strength of the magnetic field in the spectrograph was chosen such that the two breakup products were focused onto different sides of the PPAC. The counting rate due to elastic scattering of the ^{11}B beam was strongly reduced by mounting a 2 mm thick and 7 mm wide tantalum beam stop at the appropriate

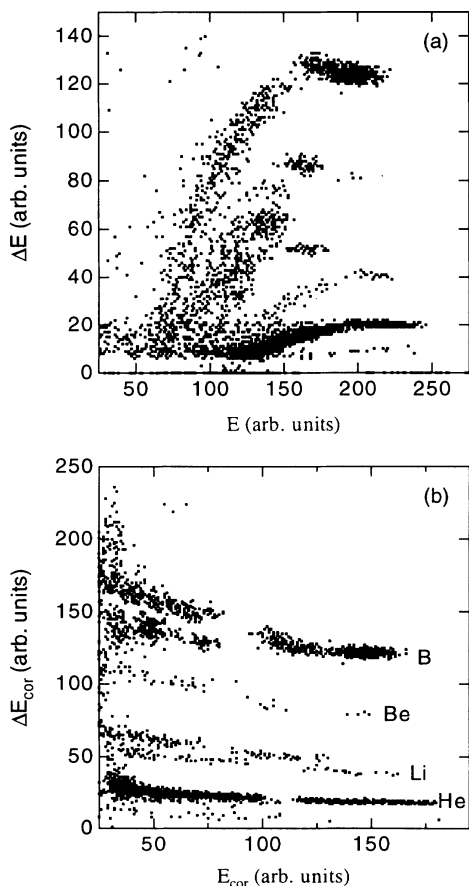


FIG. 2. (a) Measured energy deposited in the Bragg curve detector versus the pulse height of the plastic scintillator for reaction products produced in the reaction between 87 MeV ^{11}B ions and a 2.2 mg/cm 2 ^{12}C target at $\theta_{\text{lab}} = 14.2^\circ$ and incident on the high-energy end of the focal plane detector. (b) Same data as shown in (a) after applying corrections for the attenuation of the light in the scintillator and the position dependence of the energy loss of the reaction products in the Bragg curve detector. The reaction products that can be clearly identified are ^4He , $^6,^7\text{Li}$, ^9Be , and $^{10,11}\text{B}$.

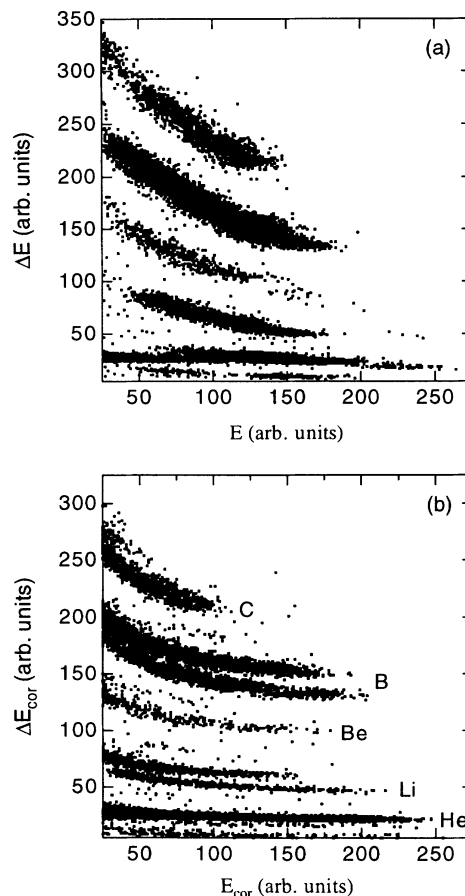


FIG. 3. (a) Measured energy deposited in the Bragg curve detector versus the pulse height of the plastic scintillator for reaction products produced in the reaction between 87 MeV ^{11}B ions and a 2.2 mg/cm 2 ^{12}C target at $\theta_{\text{lab}} = 14.2^\circ$ and incident on the low-energy end of the focal-plane detector. (b) Same data as shown in (a) after applying corrections for the attenuation of the light in the scintillator. The reaction products that can be clearly identified are ^4He , $^6,^7\text{Li}$, ^9Be , $^{10,11}\text{B}$, and ^{12}C .

location in front of the focal-plane detector system (see Fig. 1).

Particle identification was achieved by using the BCD as a ΔE detector and measuring the residual energy with the plastic scintillator. Figure 2(a) shows the energy deposited in the BCD versus the pulse height of the scintillator for particles detected on the high-energy end of the focal plane. The Z identification can be considerably improved by correcting for the attenuation of light in the scintillator and the position dependence of the energy deposited in the BCD. Both corrections can be made using the measured position along the focal plane. Figure 2(b) shows the same data as Fig. 2(a), after applying these corrections. Figure 2(b) clearly shows that both the nuclear charge and the mass of the reaction products detected on the high-energy end of the focal-plane detector can be uniquely identified. Figure 3(a) shows the energy deposited by nuclei incident on the low-energy end of the focal-plane detector versus the pulse height in the low-energy scintillator. Figure 3(b) shows the same data as Fig. 3(a) after the measured pulse height in the low-energy scintillator has been corrected for the light attenuation. Figure 3(b) clearly shows that both the nuclear charge and the mass of the reaction products detected on the low-energy end of the focal-plane detector can be uniquely identified.

III. EXPERIMENTAL RESULTS

A. Elastic scattering and inelastic scattering

Elastic-scattering cross sections were measured at several laboratory angles between 4.2° and 24.2° . The reaction products were focused onto the low-energy side of the PPAC and were identified using the measured energy loss in the low-energy side of the BCD and the measured pulse height in the low-energy side of the scintillator. The energy of the reaction products was obtained from the measured position along the focal plane. Figure 4 shows the measured Q -value spectra of ^{11}B nuclei at three different laboratory angles. The spectra are dominated by elastic scattering and inelastic scattering in which ^{12}C is excited to its 4.4 MeV first excited state. The widths of the peaks in the energy spectra are dominated by energy straggling of the beam and the reaction products in the target. The relative cross sections for elastic scattering were obtained from the measured yields and the counts in a monitor detector mounted at $\theta_{\text{lab}} = -30^\circ$ with respect to the beam. Absolute cross sections were obtained by normalizing the measured elastic-scattering yields at forward angles ($\theta_{\text{c.m.}} \leq 15^\circ$) to the results from a distorted wave Born approximation (DWBA) calculation. The measured cross sections for elastic scattering divided by the Rutherford cross sections are shown in Fig. 5(a). The solid line in Fig. 5(a) shows the results of a calculation using the code PTOLEMY [7] with

an energy-independent real and imaginary Woods-Saxon potential. The potential used ($V=60.5$ MeV, $r_0=1.09$ fm, $a=0.61$ fm, $W=36.0$ MeV, $r_{0i}=1.18$ fm, $a_i=0.45$ fm, and $r_{c0}=1.25$ fm) is taken from Ref. [8] and gives a reasonable description of the elastic-scattering data for the $^{11}\text{B}+^{12}\text{C}$ system at laboratory energies between 28.7 MeV and 76.6 MeV. The elastic-scattering cross sections calculated using this optical model potential are in reasonable agreement with the measured elastic-scattering yields, and these potential parameters are used in the DWBA calculations discussed in Sec. IV A.

The measured cross sections for inelastic-scattering reactions in which the 4.4 MeV state in ^{12}C is excited are shown as a function of the center-of-mass scattering angle in Fig. 5(b). The solid line in Fig. 5(b) shows the results of an inelastic DWBA calculation with the code PTOLEMY [7], using the optical-model potential from Ref. [8] and a $B(E2) \uparrow$ value of $0.0041 e^2 b^2$ [9]. The calculated cross sections for exciting the 4.4 MeV 2^+ state in ^{12}C are in reasonable agreement with the measured yields.

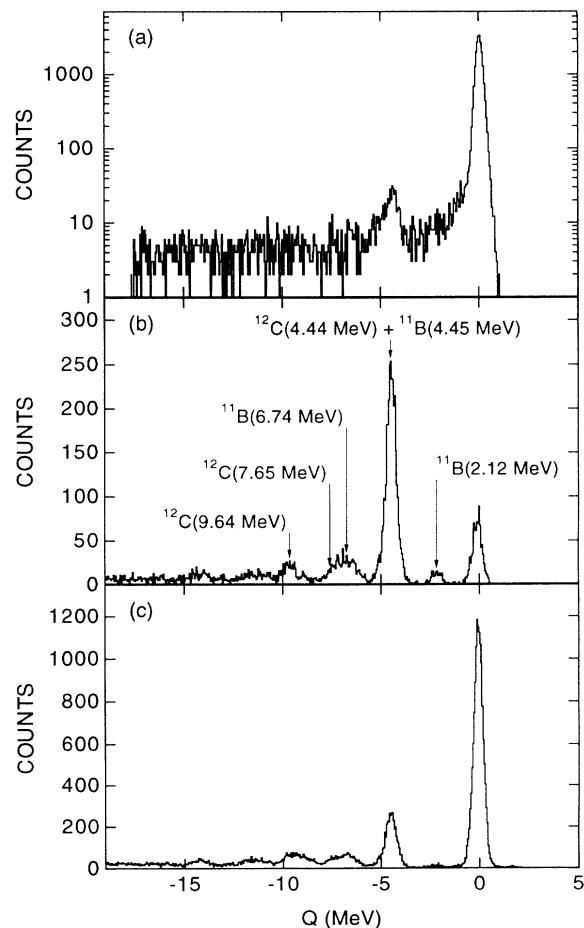


FIG. 4. Measured Q -value spectra of scattered ^{11}B ions for $^{11}\text{B}+^{12}\text{C}$ at $E_{\text{lab}}=87$ MeV and (a) $\theta_{\text{lab}} = 4.2^\circ$, (b) $\theta_{\text{lab}} = 14.2^\circ$, and (c) $\theta_{\text{lab}} = 16.7^\circ$. The location of some excited states in ^{11}B and ^{12}C are indicated in (b). Note that (a) has a logarithmic scale while (b) and (c) have linear scales.

B. Coincidence measurements

A breakup event is defined as an event in which a particle is detected on the low-energy end of the focal-plane detector in coincidence with a particle detected on the high-energy end of the focal-plane detector, within a coincidence time of 100 ns. A time-to-digital converter (TAC) is used to measure the difference in the arrival time of reaction products on the high-energy and low-energy ends of the focal-plane detector. The TAC spectrum is used to separate true coincidences from random coincidences. Almost all of the random coincidence rate

is due to α - α and α - ^{11}B coincidences. The α - ^7Li coincidences are dominated by true coincidences (random coincidences contribute at most 5% to the total α - ^7Li coincidence rate).

Particle identification is accomplished by first identifying the particle detected at the high-energy end of the focal-plane detector. The response of the high-energy end of the focal-plane detector in coincidence mode is the same as its response in singles mode. Therefore, the gates used to identify the reaction products on the high-energy end in singles mode are also used to identify the reaction products detected on the high-energy end in coincidence mode (see Fig. 2). The response of the low-energy end of the focal-plane detector in coincidence mode is different from its response in singles mode since the majority of the reaction products detected on the high-energy end of the focal-plane detector will also deposit a fraction of

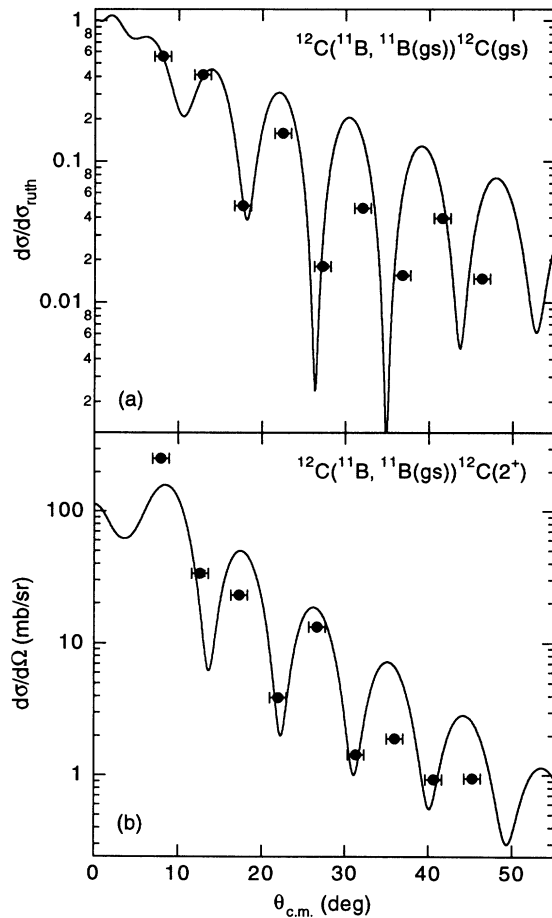


FIG. 5. (a) Measured elastic-scattering angular distributions for $^{11}\text{B}+^{12}\text{C}$ at $E_{\text{lab}}=87$ MeV. The solid curve shows the results of a DWBA calculation using the optical-model potential of Ref. [8]. The measured elastic-scattering yields at forward angles ($\theta_{\text{c.m.}} \leq 15^\circ$) were normalized to the results from the DWBA calculation. The horizontal error bars of the data points indicate the opening angle of the aperture of the spectrograph used in the measurement of the elastic-scattering angular distribution. (b) Measured inelastic-scattering angular distributions for $^{11}\text{B}+^{12}\text{C}$ at $E_{\text{lab}}=87$ MeV. The solid curve shows the results of a finite-range DWBA calculation using the optical potential of Ref. [8]. The horizontal error bars of the data points indicate the opening angle of the aperture of the spectrograph used in the measurement of the inelastic-scattering angular distribution.

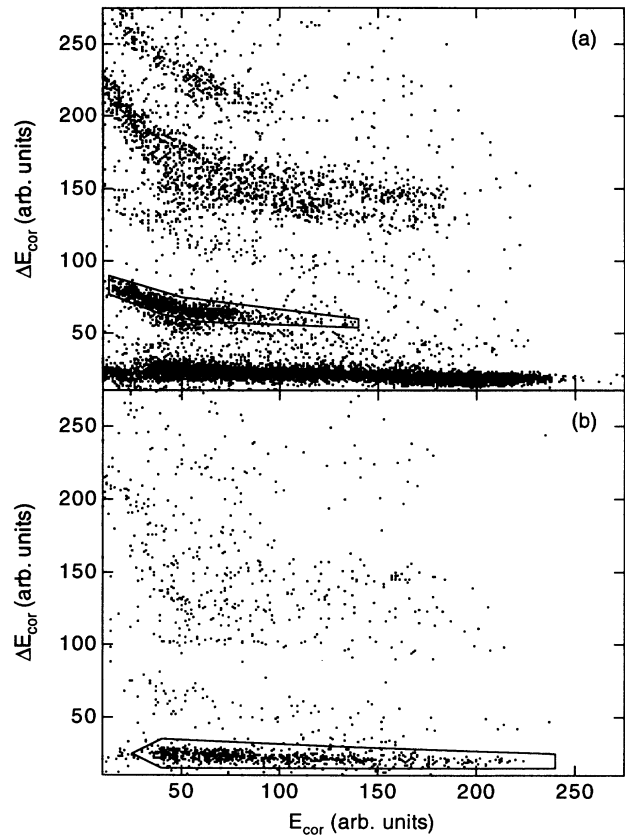


FIG. 6. (a) Measured energy loss of the ions incident on the low-energy end of the BCD (corrected for the energy deposited in the low-energy end of the BCD by the fragment detected on the high-energy end of the focal-plane detector) versus the measured pulse height in the low-energy scintillator (corrected for the light attenuation). The coincidence data shown in this figure were obtained for $^{11}\text{B}+^{12}\text{C}$ at $E_{\text{lab}}=87$ MeV and $\theta_{\text{lab}}=14.2^\circ$ and are in coincidence with a ^4He ion detected on the high-energy end of the focal-plane detector. (b) As (a), except only those events are shown that are in coincidence with a ^7Li ion detected on the high-energy end of the focal-plane detector.

their energy in the low-energy end of the BCD (see Fig. 1). Figures 6(a) and 6(b) show the measured energy loss of ions incident on the low-energy end of the BCD (corrected for the energy deposited in the low-energy end of the BCD by the fragment detected on the high-energy end of the PPAC) versus the measured pulse height in the low-energy scintillator (corrected for the light attenuation) for fragments in coincidence with ^4He and ^7Li ions incident on the high-energy end of the focal-plane detector, respectively. The gates shown in Fig. 6(a) and Fig. 6(b) are used to identify ^4He and ^7Li in the low-energy end of the focal-plane detector.

The energies of the breakup products are obtained from the measured position along the focal plane. Figure 7(a) shows the energy of the ^7Li ions detected on the low-energy side of the focal-plane detector versus the energy of the coincident ^4He ions detected on the high-energy end of the focal-plane detector. Figure 7(b) shows the total kinetic energy of the breakup fragments ($E_\alpha + E_{\text{Li}}$). This sum energy spectrum is dominated by elastic breakup (all reaction products are left in their

ground state) and inelastic breakup (in which the target recoil is left in its 4.44 MeV excited state). The resolution obtained in the sum energy spectrum is 1.0 MeV (FWHM) and is dominated by the effects of energy straggling of the beam and breakup fragments in the target. The limited energy resolution does not allow us to separate pure elastic breakup from inelastic breakup in which the ^7Li fragment is left in its 0.478 MeV $1/2^-$ first excited state. However, an analysis of $^7\text{Li}(\alpha, \alpha')$ and $^7\text{Li}(\alpha, \alpha')$ reactions by Paul *et al.* [6] showed that the breakup of $^{11}\text{B}^*$ predominantly produces ^7Li fragments in their ground state. This is crucial since the comparison between previously measured yields for radiative capture and the yields of projectile breakup can only be made for elastic breakup events. The gate used to select elastic breakup events is indicated in Fig. 7(b).

The laboratory energies of the two breakup products are used to calculate their relative energy using the formula

$$\varepsilon_{\text{rel}} = \frac{m_{\text{Li}}m_{\text{He}}}{m_{\text{He}} + m_{\text{Li}}} \left[\frac{E_{\text{He}}}{m_{\text{He}}} + \frac{E_{\text{Li}}}{m_{\text{Li}}} - 2\sqrt{\frac{E_{\text{He}}}{m_{\text{He}}} \frac{E_{\text{Li}}}{m_{\text{Li}}} \cos \theta_{\text{rel}}} \right], \quad (1)$$

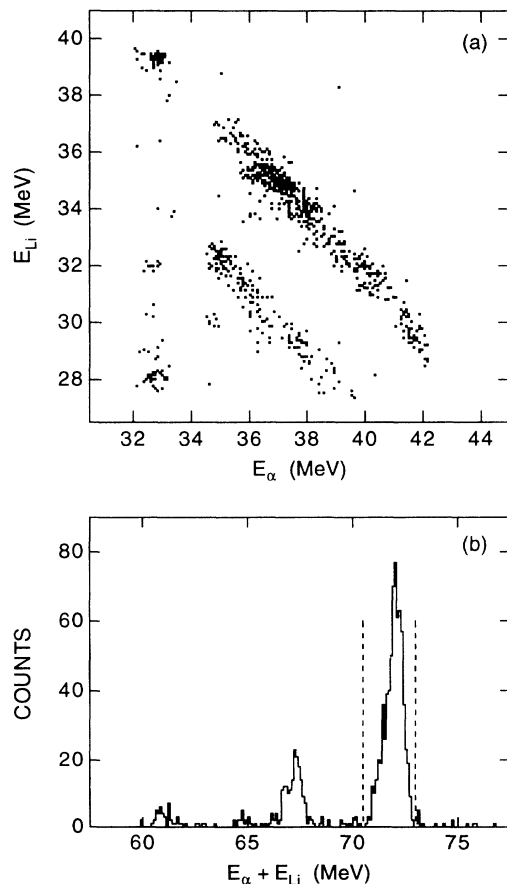


FIG. 7. (a) Energy of ^7Li ions detected on the low-energy end of the focal-plane detector versus the energy of ^4He ions detected in coincidence on the high-energy end of the focal-plane detector. Data shown were obtained for $^{11}\text{B}+^{12}\text{C}$ at $E_{\text{lab}}=87$ MeV and $\theta_{\text{lab}} = 14.2^\circ$. (b) Sum energy spectrum of the breakup fragments shown in (a). The gate shown is used to select elastic-breakup events.

where m_{He} and m_{Li} are the masses of the ^4He and ^7Li fragments, E_{He} and E_{Li} are the laboratory energies of the ^4He and ^7Li fragments, and θ_{rel} is the laboratory opening angle between the ^4He and ^7Li fragments. The laboratory energies of the breakup fragments are obtained from the measured energies after making corrections for the energy loss in the target, assuming that the breakup occurs in the center of the target. For a pinhole aperture the laboratory opening angle between the ^4He and ^7Li fragments is 0° . In our measurement the maximum laboratory opening angle that could be detected is 2.8° . Figure 8 shows histograms of the laboratory opening angle between the two breakup fragments detected in the focal plane of the spectrograph obtained from Monte Carlo simulations of the breakup of ^{11}B with $\varepsilon_{\text{rel}}=0.5$ MeV [Fig. 8(a)] and $\varepsilon_{\text{rel}}=2.0$ MeV [Fig. 8(b)]. At both energies the laboratory opening angle spectrum peaks at $\theta_{\text{rel}} = 1^\circ$, and this value of θ_{rel} has been used in the calculation of the relative energy of the breakup fragments.

Figure 9 shows a part of the relative energy spectrum of elastic breakup events obtained at $\theta_{\text{lab}} = 24.2^\circ$. The spectrum is dominated by two peaks, corresponding to the 9.19 MeV and 9.28 MeV excited states in ^{11}B . The solid curve in Fig. 9 shows a fit to the data with the sum of two Breit-Wigner line shapes. The fit parameters are listed in Table I and are compared with known properties of the 9.19 MeV and 9.28 MeV excited states in ^{11}B . The intrinsic widths of these states are very small (1.9×10^{-3} keV and 4 keV, respectively) and the measured widths (30 ± 11 keV and 37 ± 9 keV, respectively) are dominated by target effects and by the variation in opening angle of the breakup fragments entering the spectrograph due to the finite size of the aperture mounted at the entrance to the spectrograph. Monte Carlo simulations show that the relative energy resolution at $\varepsilon_{\text{rel}}=600$ keV is expected to be 41 keV, in good agreement with the measured widths.

TABLE I. Properties of peaks observed in the relative energy spectrum of ^{11}B fragments shown in Fig. 9 compared with known properties of states in ^{11}B [6,16].

Peak	Measured E_{rel} (MeV)	Measured Γ (keV)	$E_{\text{rel}} + Q_{\text{gg}}$ (MeV)	$E_{\text{ex}}(^{11}\text{B}^*)$ (MeV)	Γ (keV)
1	0.527 ± 0.010	30 ± 11	9.191 ± 0.010	9.19	1.9×10^{-3}
2	0.604 ± 0.010	37 ± 9	9.268 ± 0.010	9.28	4

Table II lists the leading factors and their calculated contributions to this resolution. The relative energy resolution obtained from this technique can be improved significantly by using thinner targets and either a smaller aperture at the entrance to the spectrograph or by employing ray-tracing techniques.

The efficiency to detect the elastic breakup fragments of ^{11}B has been studied in detail using Monte Carlo simulations. It is assumed that the breakup fragments are emitted with an isotropic distribution in the rest frame of the excited ^{11}B nucleus. These simulations include the

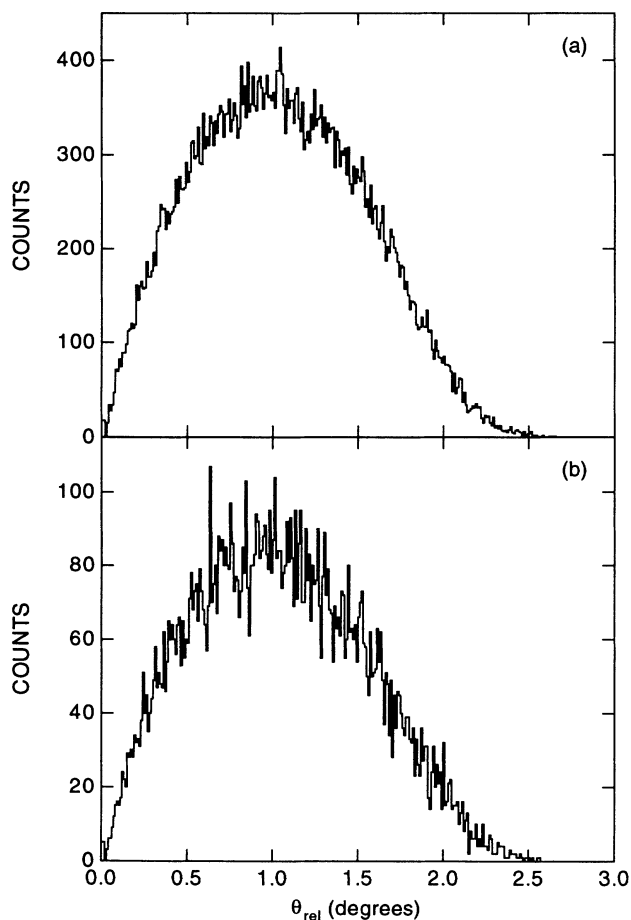


FIG. 8. Laboratory opening angle between the two breakup products obtained from Monte Carlo simulations of the breakup of 87 MeV ^{11}B with (a) $\varepsilon_{\text{rel}}=0.5$ MeV and (b) $\varepsilon_{\text{rel}}=2.0$ MeV. In both simulations 10^6 events were generated and the difference in the number of counts in spectrum (a) compared to spectrum (b) reflects the increase in detection efficiency with decreasing relative energy.

transport of the breakup products in the Enge split-pole spectrograph as well as energy loss and energy straggling of the incident beam and breakup fragments in the target. The relative energy of the breakup fragments is chosen randomly between 0 and 4 MeV. Figure 10(a) shows the reconstructed relative energy spectrum of those breakup events in which ^4He fragments are detected on the high-energy end of the focal-plane detector in coincidence with ^7Li ions detected on the low-energy end of the focal-plane detector. The gap in this spectrum between $\varepsilon_{\text{rel}}=830$ keV and $\varepsilon_{\text{rel}}=970$ keV is due to the presence of the moveable beam stop. Figure 10(b) shows the reconstructed relative energy spectrum of those breakup events in which ^7Li fragments are detected on the high-energy end of the focal-plane detector in coincidence with ^4He ions detected on the low-energy end of the focal-plane detector. For a limited range of relative energies ($120 \text{ keV} < \varepsilon_{\text{rel}} < 360 \text{ keV}$) our setup is sensitive to breakup events in which the ^7Li products move forward in the $^{11}\text{B}^*$ rest frame and breakup events in which the ^7Li products move backward in the $^{11}\text{B}^*$ rest frame. This nearly doubles the detection efficiency in this energy region and produces the “bump” in the reconstructed relative energy spectrum shown in Fig. 10(b). Figure 10(c) is the sum of the spectra shown in Fig. 10(a) and 10(b), and is used to correct the measured relative energy spectrum for variations in detection efficiency.

Absolute cross sections were obtained by correcting the data for the calculated detection efficiency, and using the normalization factor obtained from the elastic-scattering

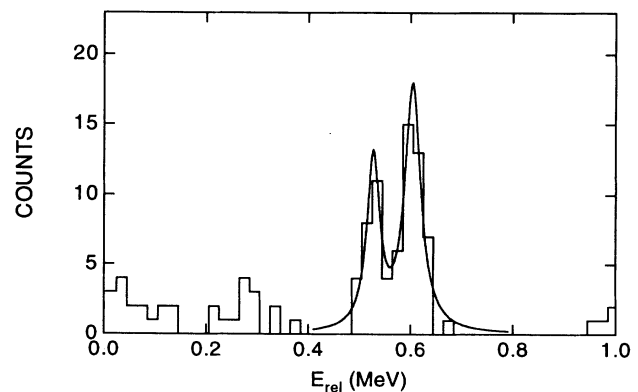


FIG. 9. Expanded section of the reconstructed relative energy spectrum of ^7Li and ^4He fragments produced in the elastic breakup of 87 MeV ^{11}B ions incident on a ^{12}C target and emitted at $\theta_{\text{lab}} = 24.2^\circ$. The solid curve shows a fit to the spectrum with two Breit-Wigner line shapes.

TABLE II. Calculated contributions to the relative energy resolution at $\varepsilon_{\text{rel}}=600$ keV.

Source	Contribution (keV, FWHM)
Energy straggling in target	36
Variation in opening angle due to aperture size	18
Intrinsic resolution of PPAC (1 mm)	8
Added in quadrature	41

data (see Sec. III A). The transformation from the laboratory to the center-of-mass frame was carried out using the reconstructed excitation energy of ^{11}B .

The variations in the intensity of the states in ^{11}B corresponding to the peaks at $\varepsilon_{\text{rel}}=0.527$ MeV and at $\varepsilon_{\text{rel}}=0.604$ MeV is dominated by variations in the detec-

tion efficiency. The fragments produced via the sequential breakup of these states are focused near the edge of the high-energy and low-energy sides of the focal-plane detector. A systematic error in the position calibration of less than 2 mm can change the calculated detection efficiency in this relative energy region by more than a factor of 5.

In the reconstruction of the relative energy of the breakup products we have neglected Coulomb acceleration effects. For particle decay via excited states in ^{11}B , the sequential breakup occurs far away from the interaction point (where the ^{11}B nucleus was excited). Consequently, the energy of the breakup products is not affected by final-state interactions with the target. However, the products from a direct-breakup reaction will experience significant Coulomb acceleration effects as was recently observed in the breakup of ^7Li by Gazes *et al.* [10,11]. These effects must be considered in studies of direct breakup and attempts to use the measured direct-breakup yields to obtain information about radiative capture cross sections.

IV. DISCUSSION

A. Sequential breakup

In a sequential breakup reaction the projectile is excited to a well-defined excited state, which subsequently particle decays. The ground state Q value for the breakup of ^{11}B into ^4He and ^7Li fragments is 8.664 MeV. Some properties of the states in ^{11}B above the breakup threshold are listed in Table III.

Figure 11 shows the measured relative energy spectra for elastic breakup obtained at $\theta_{\text{lab}} = 6.7^\circ, 14.2^\circ, 19.2^\circ,$ and 24.2° . In addition, the calculated detection efficiency is shown as a function of the reconstructed relative energy. The relative energy spectra show three pronounced peaks in the energy region below 2.5 MeV. The centroid and width of these peaks were obtained from a fit to the relative energy spectrum at $\theta_{\text{lab}} = 14.2^\circ$, assuming Breit-Wigner line shapes. The measured centroids and widths, listed in Table IV, allow these three peaks to be identified as arising from the sequential breakup of the 9.28 MeV, 10.26+10.33 MeV, and 10.60 MeV states in ^{11}B . The width of the 9.28 MeV state is limited by the experimental resolution. The widths of the 10.26 MeV and 10.33 MeV states in ^{11}B are similar to the energy difference between them. We therefore have not made any attempt to determine the relative contributions of these two states to the 10.27 MeV peak.

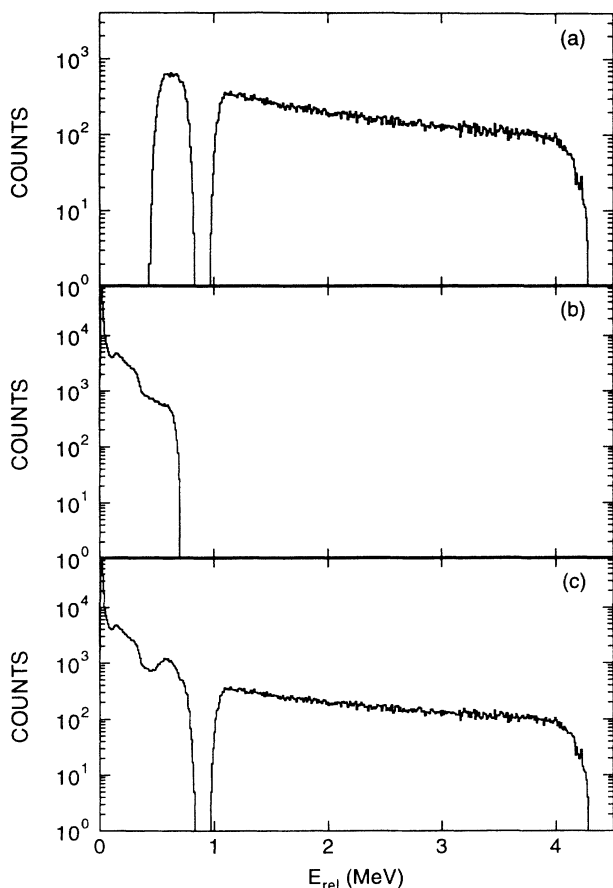


FIG. 10. (a) Reconstructed relative energy spectrum obtained from Monte Carlo simulations for those elastic breakup events in which ^4He fragments are detected on the high-energy end of the focal-plane detector in coincidence with ^7Li ions detected on the low-energy end of the focal-plane detector. The gap in this spectrum between $\varepsilon_{\text{rel}}=830$ keV and $\varepsilon_{\text{rel}}=970$ keV is due to the presence of the moveable beam stop. (b) Reconstructed relative energy spectrum obtained from Monte Carlo simulations for those elastic-breakup events in which ^7Li fragments are detected on the high-energy end of the focal-plane detector in coincidence with ^4He ions detected on the low-energy end of the focal-plane detector. (c) Sum of the reconstructed relative energy spectra shown in (a) and (b).

TABLE III. Properties of excited states in ^{11}B above the α -decay threshold.

E_{ex} (MeV)	J_π	E_{rel} (MeV)	Decay mode	Γ (keV) Ref. [17]	Γ (keV) Ref. [12]	Γ (keV) Ref. [6]	Γ_{γ_0} (eV) Ref. [6,18]
8.92	$5/2^-$	0.26	γ, α	4×10^{-3}			4.7
9.19	$7/2^+$	0.52	γ, α	1.9×10^{-3}			0.17
9.28	$5/2^+$	0.61	γ, α	4			1.15
9.87	$3/2^+$	1.21	α	110 ± 15	130 ± 30	250–290	< 0.5
10.26	$1/2^\pm, 3/2^\pm$	1.60	γ, α	150 ± 25	150 ± 40	200–433	17.0
10.33	$5/2^-, 7/2^-$	1.67	γ, α	110 ± 20	80 ± 3	100	1.0
10.60	$7/2^+$	1.94	γ, α	100 ± 20	70 ± 1	90	≤ 0.2
10.96	$5/2^-$	2.30	α	~ 4500			
11.27	$9/2^+$	2.63	α	110 ± 20			
11.44	?	2.83	α	103 ± 20			
11.59	$5/2^+$	2.96	n, α	170 ± 30			
11.89	$7/2^+$	3.15	n, α	200 ± 20			
12.00	$7/2^+$	3.35	n, α	~ 1000			

Absolute cross sections for sequential breakup of the 10.26+10.33 MeV and 10.60 MeV states in ^{11}B were obtained using Breit-Wigner fits to the efficiency-corrected data using the centroids and widths listed in Table IV as fixed parameters and the normalization factor obtained from the elastic-scattering data. The measured yields are summarized in Table V. Due to large variations in the calculated detection efficiency for sequential breakup of the 9.28 MeV state in ^{11}B as a result of small systematic errors in the position calibration (see Sec. III B), the extracted breakup yields for this state have a potentially large systematic error.

The measured angular distributions of the sequential elastic breakup of the 10.26+10.33 MeV and 10.60 MeV states are shown in Figs. 12(a) and 12(b), respectively. The measured yields are compared with the results of inelastic single-step DWBA calculations performed using the program PTOLEMY [7]. The calculations assume that the excitation is a single-step process. The calculations use $B(E\lambda)$ values calculated from the Γ_{γ_0} widths obtained from $^7\text{Li}(\alpha, \gamma)^{11}\text{B}$ radiative capture experiments [6]. Since the decay of the states observed is dominated by α decay (the threshold for neutron and proton decay is 11.45 MeV and 11.23 MeV, respectively), the cross section for exciting the states in ^{11}B is taken to be equal to the breakup cross section.

The measured angular distribution for the sequential breakup of the 10.26+10.33 MeV states as a function of the center-of-mass scattering angle of $^{11}\text{B}^*$ is shown in Fig. 12(a). The existence of two states in ^{11}B at 10.26 MeV and 10.33 MeV is inferred from studies of $^7\text{Li}(\alpha, \gamma)^{11}\text{B}$ [6], $^7\text{Li}(\alpha, \alpha')^7\text{Li}$ [12], and $^9\text{Be}(\alpha, p)^{11}\text{B}$ [13]. Possible spin assignments, obtained from an R -

matrix analysis of the $^7\text{Li}(\alpha, \gamma)^{11}\text{B}$ and $^7\text{Li}(\alpha, \alpha')^7\text{Li}$ data, are $1/2^\pm$ and $3/2^\pm$ for the 10.26 MeV state, and $5/2^-$ and $7/2^-$ for the 10.33 MeV state. The gamma widths Γ_{γ_0} were obtained by Paul *et al.* from an R -matrix analysis of the $^7\text{Li}(\alpha, \gamma)^{11}\text{B}$ data [6]. The extracted gamma widths Γ_{γ_0} are 5–17 eV and 0.9–1.0 eV for the 10.26 MeV and 10.33 MeV states, respectively. The curves in Fig. 12(a) show the results of inelastic single-step DWBA calculations. The dashed curve shows the cross sections calculated for exciting a $3/2^+$ state at 10.26 MeV with a $\Gamma_{\gamma_0}=17$ eV. It is assumed that the nuclear deformation length ($\beta_n R_n$) is equal to the Coulomb deformation length ($\beta_c R_c$). The solid curve shows the cross sections calculated for exciting a $1/2^-$ state at 10.26 MeV with a $\Gamma_{\gamma_0}=5$ eV and $\beta_n R_n = \beta_c R_c$. The dotted curve shows the cross sections calculated for exciting a $1/2^-$ state at 10.26 MeV with a $\Gamma_{\gamma_0}=5$ eV and a nuclear deformation length which is 50% smaller than the Coulomb deformation length. These calculated yields are in reasonable agreement with the measured cross sections. However, the angles at which the breakup yields are measured in this work do not allow us to verify the oscillatory nature of the calculated angular distribution. It should be noted that the calculations do not include the possibility of multistep processes. In addition, the calculation assumes that the excitation process is purely electric, even though a comparison between the measured gamma width and the Weisskopf estimate for this transition is compatible with it being an $M1$ transition. We have not considered the 10.33 MeV state in the DWBA calculations since its Γ_{γ_0} is significantly smaller than the Γ_{γ_0} of the 10.26 MeV state.

The measured angular distribution for the sequential

TABLE IV. Properties of peaks observed in the relative energy spectrum of ^4He and ^7Li fragments produced in the elastic breakup of ^{11}B fragments at $\theta_{lab} = 14.2^\circ$ compared with known properties of states in ^{11}B [6,16].

Peak	Measured E_{rel} (MeV)	Measured Γ (keV)	$E_{rel} + Q_{gg}$ (MeV)	E_{ex} ($^{11}\text{B}^*$) (MeV)	Γ ($^{11}\text{B}^*$) (keV)
1	0.604 ± 0.010	37 ± 9	9.268 ± 0.010	9.28	4
2	1.610 ± 0.014	337 ± 44	10.274 ± 0.014	10.26+10.33	150–433
3	1.948 ± 0.007	83 ± 22	10.612 ± 0.007	10.60	70–100

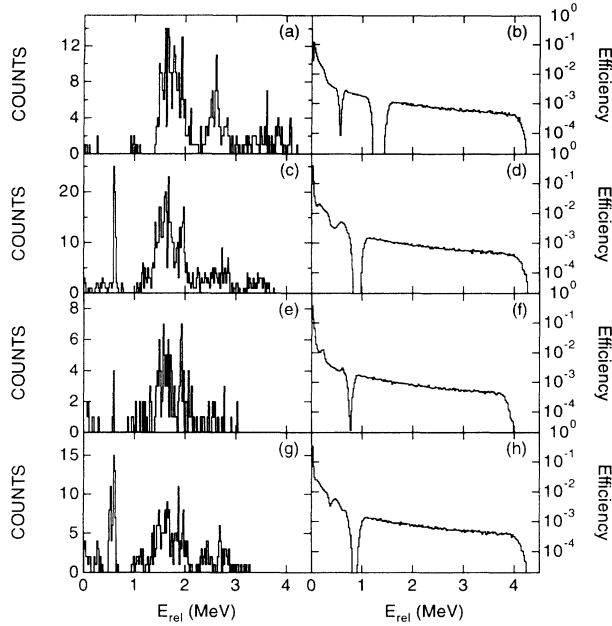


FIG. 11. Measured relative energy spectra obtained for the elastic breakup of 87 MeV ^{11}B ions incident on a ^{12}C target into ^4He and ^7Li fragments at (a) $\theta_{\text{lab}} = 6.7^\circ$, (c) $\theta_{\text{lab}} = 14.2^\circ$, (e) $\theta_{\text{lab}} = 19.2^\circ$, and (g) $\theta_{\text{lab}} = 24.2^\circ$. The calculated detection efficiency is shown as a function of the reconstructed relative energy at (b) $\theta_{\text{lab}} = 6.7^\circ$, (d) $\theta_{\text{lab}} = 14.2^\circ$, (f) $\theta_{\text{lab}} = 19.2^\circ$, and (h) $\theta_{\text{lab}} = 24.2^\circ$.

breakup of the 10.60 MeV state as a function of the center-of-mass scattering angle of $^{11}\text{B}^*$ is shown in Fig. 12(b). The existence of this state is inferred from studies of $^7\text{Li}(\alpha, \alpha')^7\text{Li}$ [12] and $^9\text{Be}(\alpha, p)^{11}\text{B}$ [13]. This state was not clearly observed in the $^7\text{Li}(\alpha, \gamma_0)^{11}\text{B}$ reaction [6] and Paul *et al.* could only determine an upper limit of 0.2 eV for the gamma width Γ_{γ_0} . The curve in Fig. 12(b) shows the results of an inelastic single-step DWBA calculation in which the electromagnetic transition strength is adjusted and the nuclear deformation length is assumed to be equal to the Coulomb deformation length. The shape of the calculated angular distribution is in reasonable agreement with the measured angular distribution. The gamma width Γ_{γ_0} used in the DWBA calculation is 2×10^{-5} eV.

TABLE V. Measured cross sections for sequential breakup of ^{11}B into ^4He and ^7Li fragments as a function of scattering angle for the two strongest states in ^{11}B observed in this experiment.

θ_{lab}	10.26+10.33 MeV (mb/sr)	10.60 MeV (mb/sr)
6.7°	1.86 ± 0.20	0.32 ± 0.08
14.2°	0.68 ± 0.04	0.16 ± 0.02
19.2°	0.27 ± 0.03	0.074 ± 0.017
24.2°	0.13 ± 0.01	0.027 ± 0.006

B. Future breakup studies

The detector system described in this paper is also being used to study the breakup of ^{16}O into ^{12}C and ^4He fragments. The time-reversed process, radiative capture of ^{12}C and ^4He , is important for the understanding of the He-burning phase in stars and their subsequent evolution [14,15]. However, at astrophysical energies ($E_{\text{c.m.}} \approx 300$ keV) the cross section is much too small to be measured directly by present techniques. Estimates of the cross section for this process have relied heavily on extrapolation of measurements carried out in the energy region above $E_{\text{c.m.}} = 1$ MeV. Due to the large breakup Q value (7.162 MeV) the velocity of the scattered ^{16}O beam is sufficiently different from the velocities of the breakup fragments so that the scattered ^{16}O ions are focused onto a different region of the focal-plane detector. Fig.

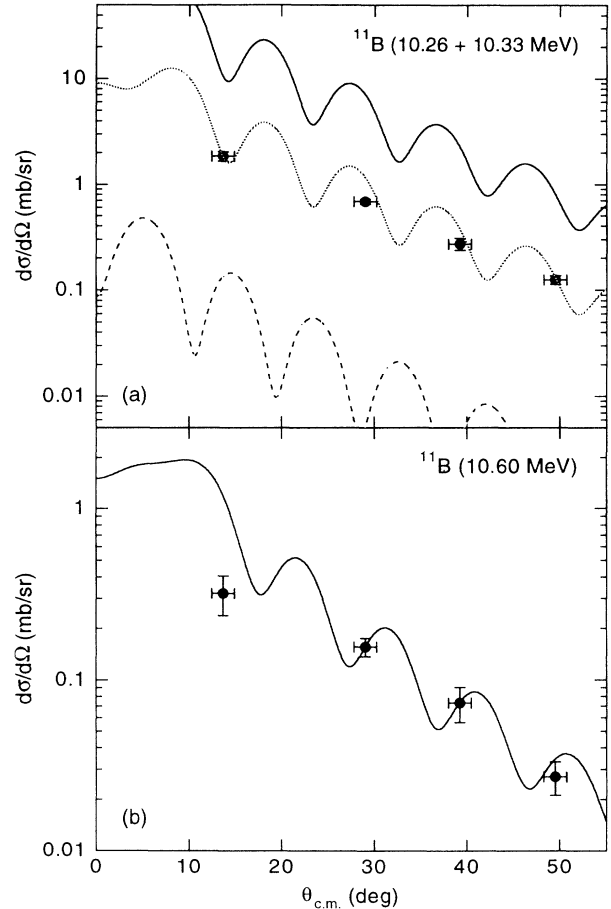


FIG. 12. (a) Measured sequential elastic breakup cross sections of the 10.26+10.33 MeV states in ^{11}B as a function of the center-of-mass scattering angle of $^{11}\text{B}^*$. The curves show the results of single-step DWBA calculations which are discussed in the text. (b) Measured sequential elastic-breakup cross sections of the 10.60 MeV state in ^{11}B as a function of the center-of-mass scattering angle of $^{11}\text{B}^*$. The curve shows the results of a single-step DWBA calculation which is discussed in the text.

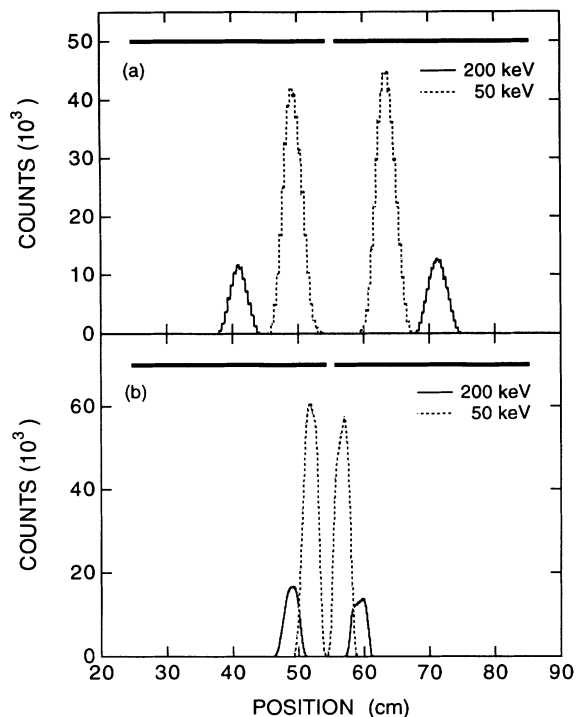


FIG. 13. Results of Monte Carlo simulations of elastic breakup of 125 MeV ^{16}O incident onto a 2.2 mg/cm^2 ^{12}C target with $\epsilon_{\text{rel}}=50 \text{ keV}$ and $\epsilon_{\text{rel}}=200 \text{ keV}$. (a) A position spectrum of the ^4He ions detected in coincidence with ^{12}C nuclei in the focal plane of the spectrograph. The two solid lines on the top of the figure indicate the position of the two segments of the focal-plane detector. (b) A position spectrum of the ^{12}C ions detected in coincidence with ^4He nuclei in the focal plane of the spectrograph. The two solid lines on the top of the figure indicate the position of the two segments of the focal plane detector.

ure 13 shows position spectra of ^4He and ^{12}C fragments obtained from Monte Carlo simulations of the breakup of ^{16}O into ^{12}C and ^4He with $\epsilon_{\text{rel}}=50 \text{ keV}$ (dashed histogram) and $\epsilon_{\text{rel}}=200 \text{ keV}$ (solid histogram). The magnetic field in the spectrograph was chosen such that ^{12}C and ^4He fragments with $\epsilon_{\text{rel}}=0 \text{ keV}$ were focused onto the center of the focal-plane detector. Figure 13 clearly

shows that for relative energies above 50 keV the two reaction products are well separated.

V. SUMMARY

The breakup of 87 MeV ^{11}B ions incident on a ^{12}C target into ^4He and ^7Li fragments has been studied using an Enge split-pole spectrograph and a segmented focal-plane detector. The relative energy spectra of elastic breakup events are dominated by the sequential breakup of the 9.28 MeV, 10.26+10.33 MeV, and 10.60 MeV excited states in ^{11}B . The relative energy resolution achieved with the spectrograph technique is $\sim 40 \text{ keV}$ (FWHM) and is dominated by energy straggling of the beam and the breakup products in the target. The widths of the states observed in the reconstructed relative energy spectrum are consistent with the known widths of the corresponding states in ^{11}B . Absolute cross sections can be extracted from the observed yields after taking into account the energy-dependent detection efficiency and making a normalization constant obtained from the measured elastic-scattering angular distribution. The shapes of the measured angular distributions for the sequential breakup channels are consistent with the shapes of the angular distributions obtained from single-step, inelastic DWBA calculations. The magnitudes of the calculated cross sections are rather uncertain due to ambiguities in the spin-parity assignment and/or radiation widths of the states in ^{11}B , making it difficult to make a direct comparison between the calculated and measured breakup cross sections. The technique described in this paper is also being used to study the breakup of ^{16}O into ^4He and ^{12}C at relative energies down to 50 keV. The relative energy resolution that can be achieved for that reaction is estimated to be 30 keV (FWHM).

ACKNOWLEDGMENTS

The efforts of the operation crew of the tandem accelerator of the Nuclear Structure Research Laboratory to provide us with high quality ^{11}B beams are gratefully acknowledged. We appreciate the comments we received from Dr. S. B. Gazes and Dr. K. E. Rehm on the first draft of this paper. This work was supported by a grant from the National Science Foundation.

- [1] G. Bauer, C. A. Bertulani, and H. Rebel, Nucl. Phys. **A458**, 188 (1986).
- [2] H. Utsunomiya, W. Lui, and R. P. Schmitt, Nucl. Instrum. Methods **A278**, 744 (1989).
- [3] H. Utsunomiya, Y. Lui, D. R. Haenni, H. Dejbakhsh, L. Cooke, B. K. Srivastava, W. Turmel, D. O'Kelly, R. P. Schmitt, D. Shapira, J. G. d. Campo, A. Ray, and T. Udagawa, Phys. Rev. Lett. **65**, 847 (1990).
- [4] H. Utsunomiya, R. P. Schmitt, Y. Lui, D. R. Haenni, H. Dejbakhsh, L. Cooke, P. Heimberg, A. Ray, T. Tamura, and T. Udagawa, Phys. Lett. B **211**, 24 (1988).
- [5] F. L. H. Wolfs, D. C. Bryan, K. L. Kurz, D. M. Herrick, P. A. A. Perera, and C. A. White, Nucl. Instrum. Methods **A317**, 221 (1992).
- [6] P. Paul, N. G. Puttaswamy, and D. Kohler, Phys. Rev. **164**, 1332 (1967).
- [7] S. C. Pieper, M. H. Macfarlane, and M. Rhoades-Brown, PTOLEMY. A Program for Heavy-ion Direct-reaction Calculations, Argonne National Laboratory Report No. ANL-76-11, 1976 (unpublished).
- [8] S. Albergo, S. Costa, R. Potenza, J. Romanski, C. Tuvé, L. Jarczyk, B. Kamys, A. Magiera, A. Strzalkowski, R.

- Barna, V. D'Amico, D. D. Pasquale, and G. Mannino, *Phys. Rev. C* **43**, 2704 (1991).
- [9] S. Raman, C. H. Malarkey, W. T. Milner, J. C. W. Nestor, and P. H. Stelson, *At. Data Nucl. Data Tables* **36**, 1 (1987).
- [10] S. B. Gazes, J. E. Mason, R. B. Roberts, and S. G. Teichmann, *Phys. Rev. Lett.* **68**, 150 (1992).
- [11] J. E. Mason, S. B. Gazes, R. B. Roberts, and S. G. Teichmann, *Phys. Rev. C* **45**, 2870 (1992).
- [12] R. Y. Cusson, *Nucl. Phys.* **86**, 481 (1966).
- [13] B. Zwiegliniski, W. Benenson, G. M. Crawley, S. Gales, and D. Weber, *Nucl. Phys.* **A389**, 301 (1982).
- [14] W. D. Arnett and F. Thielemann, *Astrophys. J.* **295**, 589 (1985).
- [15] F. Thielemann and W. D. Arnett, *Astrophys. J.* **295**, 604 (1985).
- [16] G. A. Jones, C. M. P. Johnson, and D. H. Wilkinson, *Philos. Mag.* **43**, 796 (1959).
- [17] F. Ajzenberg-Selove, *Nucl. Phys.* **A506**, 1 (1990).
- [18] G. Hardie, B. W. Filippone, A. J. Elwyn, M. Wiescher, and R. E. Segel, *Phys. Rev. C* **29**, 1199 (1984).